Macro-scale grid-based and subbasin-based hydrologic modeling: joint simulation and cross-calibration

Xuefeng Chu, Zhulu Lin, Mohsen Tahmasebi Nasab, Lan Zeng, Kendall Grimm, Mohammad Hadi Bazrkar, Ning Wang, Xingwei Liu, Xiaodong Zhang and Haochi Zheng

ABSTRACT

Watershed hydrologic models often possess different structures and distinct methods and require dissimilar types of inputs. As spatially-distributed data are becoming widely available, macro-scale modeling plays an increasingly important role in water resources management. However, calibration of a macro-scale grid-based model can be a challenge. The objective of this study is to improve macro-scale hydrologic modeling by joint simulation and cross-calibration of different models. A joint modeling framework was developed, which linked a grid-based hydrologic model (GHM) and the subbasin-based Soil and Water Assessment Tool (SWAT) model. Particularly, a two-step cross-calibration procedure was proposed and implemented: (1) direct calibration of the subbasin-based SWAT model using observed streamflow data; and (2) indirect calibration of the grid-based GHM through the transfer of the well-calibrated SWAT simulations to the GHM. The joint GHM-SWAT modeling framework was applied to the Red River of the North Basin (RRB). The model performance was assessed using the Nash–Sutcliffe efficiency (NSE) and percent bias (PBIAS). The results highlighted the feasibility of the proposed cross-calibration strategy in taking advantage of both model structures to analyze the spatial/temporal trends of hydrologic variables. The modeling approaches developed in this study can be applied to other basins for macro-scale climatic-hydrologic modeling.

Key words | cross-calibration, grid-based modeling, hydrologic modeling, joint simulation Red River of the North Basin, subbasin-based modeling, SWAT

Xuefeng Chu (corresponding author)
Mohsen Tahmasebi Nasab
Lan Zeng
Kendall Grimm
Mohammad Hadi Bazrkar
Ning Wang
Xingwei Liu
Department of Civil and Environmental
    Engineering,
North Dakota State University,
P.O. Box 6050, Fargo, ND 58108-6050,
USA
E-mail: *xuefeng.chu@ndsu.edu*

Zhulu Lin
Department of Agricultural and Biosystems
    Engineering,
North Dakota State University,
P.O. Box 6050, Fargo, ND 58108-6050,
USA

Xiaodong Zhang
Haochi Zheng
Department of Earth System Science and Policy,
University of North Dakota,
Grand Forks, ND 58202-6089,
USA

INTRODUCTION

The complexity and heterogeneity of hydrologic interactions over a wide range of spatial and temporal scales (Blöschl & Sivapalan 1995) are one of many challenges in advancing our understanding of the hydrologic cycle. An example of these complexities is how the climate change and land use change affect the hydrologic cycle at various scales (Blöschl et al. 2007). The scales at which the hydrologic processes are investigated depend on the issues to be addressed. Therefore, an increasing need for representing hydrologic processes at different scales has led to three general model classifications: micro-, meso-, and macro-scale hydrologic models. The differences across these three scales demonstrate the trade-offs between spatial capability and complexity of the models.

Micro-scale models take advantage of numerical methods to discretize the space domain into a large number of small cells to provide detailed modeling and in-depth understanding of specific hydrologic processes over relatively small areas. For example, Chu et al. (2013) developed a puddle-to-puddle (P2P) modeling system to

simulate micro-scale puddle filling, spilling, merging, and splitting processes dynamics on depression-dominated surfaces. Clearly, intensive high-resolution data are required for such micro-scale modeling. Meso-scale models are developed for simulating dominant hydrologic processes in local watersheds. In a typical meso-scale model, a watershed can be divided into a number of subbasins that are well connected to the channelized drainage system in a semi-distributed fashion.

In contrast, macro-scale models can be associated with regional, continental, or even global scales and they often involve simulations of large-scale climatic and hydrologic processes. The complexity of a macro-scale model varies, mainly depending on data availability, computational resources, and research purposes. Unlike the micro- and meso-scale models, the concept of macro-scale modeling is relatively new (Sood & Smakhtin 2015). Macro-scale models offer a holistic view of hydrologic processes that can be applied for interconnected modeling of Earth systems and climate impact assessments (Gudmundsson *et al.* 2012a). Increasing availability of remote sensing datasets, high-performance computing resources, and improved representations of hydrologic processes are among the key factors that have contributed to the constant development of macro-scale models (Paiva *et al.* 2011). The capabilities, limitations, and uncertainties of macro-scale modeling have been investigated before (e.g. Döll *et al.* 2008; Gudmundsson *et al.* 2012b; Sood & Smakhtin 2015). For example, Döll *et al.* (2008) highlighted the advances, difficulties, and research perspectives associated with macro-scale modeling, and indicated that the results from macro-scale models are sensitive to: (1) uncertainties in input data due to measurement, interpolation, and other factors; (2) spatial and temporal discretization and the information density of input data; and (3) model structure.

Two approaches are commonly used for large-scale hydrologic modeling: (1) subbasin-based and (2) grid-based. Concerning the second modeling type, for instance, a grid-based structure has been adopted in macro-scale models such as the variable infiltration capacity model (Liang *et al.* 1994), the grid-to-grid model (Bell *et al.* 2007), and the California basin characterization model (Flint *et al.* 2013), where hydrologic processes are simulated for all grids separately. Tesfa *et al.* (2014) compared the scalability of surface runoff generation by employing both

subbasin-based and grid-based discretization approaches for spatial resolutions of 0.125, 0.25, 0.5, and 1°, indicating that the subbasin-based approach performed better than the grid-based approach, especially for mountainous areas in winters. In addition, calibration and validation of a macro-scale grid-based model by using streamflow data are a challenge because the point-scale streamflow data measured at gauging stations may not be directly used for such purposes. The macro-scale grid-based models require grid-based hydrologic parameters, which are not normally available or measured to be used in the calibration process. Therefore, some parameter regionalization techniques have been developed (e.g. Samaniego *et al.* 2010) to specify the localized parameters for a group of grids in macro-scale models.

Given the importance of the calibration process of the macro-scale models and to deal with this issue, the main objective of this study is to improve calibration of a macro-scale hydrologic model by proposing a macro-scale modeling framework that links a grid-based hydrologic model (GHM) and a subbasin-based model (i.e. Soil and Water Assessment Tool (SWAT)) for joint simulation and cross-calibration of different models. In this framework, a two-step cross-calibration procedure is also developed. That is, the subbasin-based SWAT model is first calibrated directly by using observed streamflow data. Then, the calibration of the grid-based GHM is indirectly performed by comparing the hydrologic variables simulated by both grid- and subbasin-based models through information transfer between grids and subbasins of the two models. The modeling methodology proposed in this study is tested by an application in the Red River of the North Basin (RRB). Table 1 lists all acronyms used (e.g. GHM, SWAT, and RRB) and their descriptions.
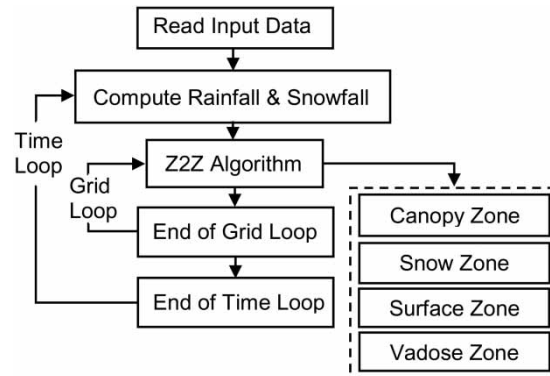
MATERIALS AND METHODS

Grid-based hydrologic model

In this study, a GHM was developed for daily macro-scale simulation of hydrologic processes. Figure 1 shows the overall modeling structure, which consists of two main loops: a grid loop and a time loop. Each grid (a basic spatial unit)

Table 1 │ List of acronyms

Acronym	Complete form
CN	Curve Number
DEM	Digital Elevation Model
G2G	Grid-to-Grid
GA	Green-Ampt
GHM	Grid-based Hydrologic Model
HRU	Hydrologic Response Unit
HUC	Hydrologic Unit Code
LAI	Leaf Area Index
LULC	Land Use Land Cover
NLCD	National Land Cover Database
NOAA	National Oceanic and Atmospheric
NSE	Nash-Sutcliffe efficiency
P2P	Puddle-to-Puddle modeling system
PBIAS	Percent Bias
PPR	Prairie Pothole Region
PRISM	Parameter-elevation Regressions on Independent Slopes Model
RRB	Red River Basin
SMA	Soil Moisture Accounting
STATSGO	State Soil Geographic dataset
SUFI2	Sequential Uncertainty Fitting, version 2
SWAT	Soil and Water Assessment Tool
SWAT-CUP	SWAT Calibration and Uncertainty Program
SWC	Soil Water Content
SWE	Snowpack Water Equivalent
TWS	Topsoil Water Storage
USDA	United States Department of Agriculture
USGS	United States Geological Survey
Z2Z	Zone-to-Zone

Figure 1 │ Simplified structure of the grid-based hydrologic model (GHM) (Z2Z: zone-to-zone algorithm).

includes four zones along a profile (i.e. canopy zone, snow zone, surface zone, and vadose zone) (Figure 1). The vadose zone is further divided into three sub-zones (topsoil, root zone, and deep vadose zone). A grid-to-grid (G2G) modeling procedure is implemented at each time step. Within each grid, a zone-to-zone (Z2Z) algorithm (Figure 1) is used to simulate hydrologic processes that vary in a fashion of Z2Z and G2G. The grid-based, bucket-type GHM requires fewer calibration parameters and is efficient in computation. It is particularly suitable for using grid-formatted climatic and hydrologic data. Since most spatially-distributed input data

(e.g. rainfall, temperature, land use/land cover (LULC), soil types) may not be available at the same grid scale or resolution, the GHM has a flexible structure that allows users to input gridded data with different resolutions.

The GHM simulates the rainfall-runoff and snowfall-snowmelt processes that are differentiated by a daily mean temperature threshold. In the canopy zone, leaf area index (LAI) is used to partition rainfall into canopy rainfall and direct surface rainfall. In the snow zone, the snowmelt process is simulated by employing the degree-day method in which snowmelt begins when the daily mean temperature is higher than a base temperature. In the surface zone, the curve number (CN) method (USDA 1986) is used to simulate rainfall excess and infiltration, which are linked to the topsoil of the vadose zone. The CN is consistently adjusted based on the water content of the topsoil over the entire simulation period. The CN is also modified by the frozen soil temperature using the approach suggested by Mohammed *et al.* (2013). In addition, surface depression storage determined by a delineation algorithm is taken into account in the model. To simulate soil moisture content and soil water movement in the vadose zone, the soil moisture accounting (SMA) method (Bennett 1998) is used for the three sub-zones (i.e. topsoil, root zone, and deep vadose zone). The potential evapotranspiration is simulated using the temperature-based method developed by Hargreaves & Samani (1985). Based on the estimated potential evapotranspiration, the actual crop evapotranspiration is then computed using the crop coefficients (Allen *et al.* 1998). In the modeling of evaporation/evapotranspiration, the water sequentially comes from the

canopy zone, surface zone, and vadose zone (including the topsoil and root zone), depending on water availability.

Introduction to SWAT

SWAT has been widely used for watershed-scale modeling and assessment of water quantity and quality. In particular, ArcSWAT (Winchell *et al.* 2013) has been developed and incorporated into ArcGIS (ESRI 2011) as an extension, which provides a user-friendly interface for digital elevation model (DEM)-based watershed delineation, state-of-the-art processing of land use and soil data, HRU (i.e. hydrologic response unit) definition, meteorological data analysis, and preparation of SWAT input files. A variety of modified SWAT models have also been developed to cope with different complex conditions in real applications (e.g. Krysanova & Arnold 2008; Douglas-Mankin *et al.* 2010). In the current study, ArcSWAT was utilized for model setup.

In SWAT, a watershed is generally divided into a number of subbasins, each of which can be further divided into many HRUs to account for heterogeneity and variability in land covers, soil types, and topography (slopes) in a subbasin. Various hydrologic processes such as surface runoff, infiltration, and groundwater flow are simulated for all HRUs. The HRU-level simulations are then integrated to generate subbasin-level simulations, which are finally routed throughout the drainage network of the entire watershed.

Delineation of a watershed and definition of HRUs require the DEM of the watershed, as well as distributions of LULC and soil types. In addition, meteorological data (e.g. precipitation, temperature, and solar radiation) are needed for model setup. In SWAT, rainfall and snowfall are determined based on a user-defined threshold temperature and utilized to simulate surface runoff, snowmelt, infiltration, and other hydrologic processes. The snowmelt process is simulated using the degree-day method, in which snowmelt is a function of air and snow temperature, melting rate, and areal coverage of snow (Neitsch *et al.* 2011). Surface runoff and infiltration are modeled by using either the CN method (USDA 1986) or the Green-Ampt (GA) method (Green & Ampt 1911). The former (i.e. the CN method) is used for daily modeling, while the latter (the GA method) is capable of providing sub-daily simulations. Three options are available in SWAT to estimate potential evapotranspiration (Neitsch *et al.* 2011): Penman–Monteith method (Monteith 1965), Priestley–Taylor method (Priestley & Taylor 1972), and Hargreaves method (Hargreaves & Samani 1985). In SWAT, soil moisture is simulated for all layers and soil water routing is performed, which involves water movement along different pathways such as plant uptake, lateral interflow, and vertical percolation. Simple mass balance equations are used to account for groundwater flow in both shallow and deep aquifers.

Study area

The RRB extends from the south of Wahpeton, North Dakota and Breckenridge, Minnesota, crossing the USA–Canada border, to Winnipeg, Manitoba in Canada (Figure 2(a) and 2(b)). The Red River combines with Assiniboine River in Winnipeg and flows into Lake Winnipeg. The RRB has a drainage area of 116,500 km^2, out of which 103,600 km^2 is located in the USA (Red River Basin Board 2000), where it drains parts of North Dakota, Minnesota, and South Dakota (Figure 2(b)).

The Red River Valley is the central part of the RRB, which has one of the most fertile soils in North America. According to the National Land Cover Database (NLCD) (Fry *et al.* 2011), nearly 60% of the RRB within the USA is covered by cultivated croplands, and the developed areas are only 4.6% of the basin area. Lacustrine soil is the dominant soil type (Jin *et al.* 2008). Also, a major part of the basin belongs to the Prairie Pothole Region (PPR) of North America (Habtezion *et al.* 2016; Tahmasebi Nasab *et al.* 2017). The slope of the basin varies from 0.04 to 0.25 m/km (Lin *et al.* 2015), which makes the RRB very flat and susceptible to frequent flooding. Figure 2(c) depicts the RRB's elevation drop from its headwaters in Wahpeton to a downstream point in Winnipeg. The 65-m elevation difference between these two locations over an 800-km river accentuates the flat topography of the RRB.

The annual mean precipitation and temperature of the basin are 500 mm and 4.3 °C, respectively (Jin *et al.* 2008; Lin *et al.* 2015). Precipitation mainly occurs between mid-May and mid-September, partly overlapping the snowmelt period at the beginning and contributing to the spring flooding condition. According to the National Weather Service Flood Stage (Galloway *et al.* 2011),
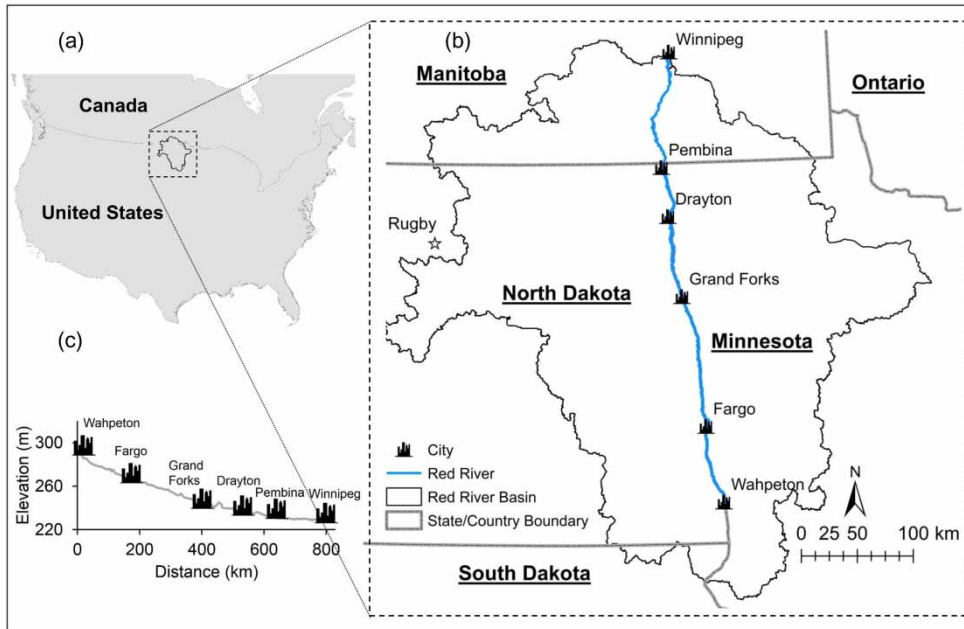
Figure 2 │ (a) and (b) Geographical location of the RRB and (c) elevation drop along the Red River from Wahpeton, North Dakota to Winnipeg, Manitoba.

overtopping of the Red River occurred 47 times during the past 108 years (occurred every year from 1993 to 2011). The key factors that make the RRB prone to flooding are: (1) basin slope, (2) soil type, (3) north-flowing direction, and (4) simultaneous snowmelt and heavy precipitation during the spring (Schwert 2009; Stadnyk *et al.* 2016).

Model setup and input data

According to the USGS hydrologic unit code (HUC), river basins in the USA are delineated and mapped by using a

hierarchical system of nested hydrologic units at different scales. In the SWAT model in this study, the RRB was divided into 178 HUC-10 subbasins ranging from 159.5 to 1,038.7 km^2. In the GHM, the study area was divided into 6,351 4×4 km grids, based on the availability of main gridded input data (e.g. precipitation and temperature). Table 2 lists the major input data and their sources for setting up the SWAT model and the GHM. The daily gridded (4×4 km^2) precipitation and minimum and maximum temperature data used in the GHM were obtained from the Parameter-elevation Regressions on Independent Slopes

Table 2 │ Summary of the major input data and their sources used for the development of the SWAT model and the grid-based hydrologic model (GHM)

Type	Source	Reference/website
Digital Elevation Model (DEM)	National Map Viewer	https://viewer.nationalmap.gov/viewer/
Land Use and Land Cover (LULC)	National Land Cover Database	Fry *et al.* (2011) www.mrlc.gov/nlcd2006.php
Soils	US General Soil Map (STATSGO2)	NRCS (2017) https://websoilsurvey.sc.egov.usda.gov
Solar Radiation	National Centers for Environmental Prediction's Climate Forecast System Reanalysis (CFSR)	Dile & Srinivasan (2014) https://globalweather.tamu.edu/
Daily Precipitation, Max, Min, and Mean Temperatures	1. Parameter-elevation Regressions on Independent Slopes Model (PRISM) 2. National Oceanic and Atmospheric Administration (NOAA)	Daly *et al.* (2008, 2015) http://prism.oregonstate.edu/ www.ncdc.noaa.gov

Model (PRISM) (Daly *et al.* 2008, 2015). In addition, daily precipitation and minimum and maximum temperature data from 12 NOAA weather stations were also obtained and used in the SWAT model. These datasets were compared to ensure that they were consistent in both models.

Soil layers and their physical characteristics play a significant role in simulating vadose zone processes. Soil type distribution was retrieved from the Digital General Soil Map of the United States or STATSGO2 (NRCS 2017). Based on the STATSGO2 data, 25 different soil types were identified in the study area. However, SWAT reclassifies the original soil data and merges similar soil types together to create a modified soil map. Similarly, to use the STATSGO2 data in the GHM, original soil data were reclassified into nine different soil types, indicating that 44% of the study area is covered by loams and only 1.7% of the area is covered by sandy clay loams. Table 3 lists the soil hydraulic property parameters for the nine soil types. These parameters include saturated hydraulic conductivity (K_s), capillary head (h_s), saturated water content (θ_s), field capacity (θ_{FC}), wilting point (θ_p), residual water content (θ_r), and soil water retention parameters (n and α).

LULC data were obtained from the NLCD (Fry *et al.* 2011). The original LULC data were reclassified into 15 categories (including open water, open space developed, low intensity developed, medium intensity developed, high intensity developed, barren land, deciduous forest, evergreen forest, mixed forest, shrub/scrub, herbaceous, hay/pasture, cultivated crops, woody wetlands, emergent herbaceous wetlands) that were incorporated into the GHM. Similarly,

SWAT reclassified the original LULC data into 15 categories. The LAI and canopy interception storage capacity values for the study area were obtained from Hasan *et al.* (2014) and Suárez (2005), respectively, and used for different LULC classes. In addition, crop coefficient (Kc) estimates for different LULC classes were extracted from Allen *et al.* (1998) for three different growth stages, namely, Kc_{ini} for the initial stage in spring, Kc_{mid} for the middle stage in summer, and Kc_{end} for the end stage in fall and winter.

Using the 30-m DEM of the RRB, surface depressions were identified by employing a simple topography-based delineation method suggested by Planchon & Darboux (2002). As a result, 39 depressional zones were included in the GHM. In the delineation process, depressions and their storage values were determined for each zone separately. Considering the existence of spurious pits or artifacts of the DEM, a special effort was made to remove those spurious pits and the adjusted depressional data were generated. In the GHM, the maximum depth of depression storage over a grid was used for each depressional zone.

Figure 3 depicts the required steps for the joint simulation and cross-calibration of the GHM. After all input data are prepared (as described above), the basin is delineated into subbasins and HRUs for the SWAT modeling and grids for the GHM modeling. Then, both models are applied to the RRB and auto-calibration is performed for the SWAT model (Figure 3). Eventually, using the calibrated SWAT results, the GHM is cross-calibrated (Figure 3). The cross-calibration process and the selected calibration parameters for both models are detailed as follows.

Table 3 │ Soil hydraulic property parameters used in the grid-based hydrologic model (Rawls *et al.* 1982; Rawls & Brakensiek 1983; Maidment 1993; Carsel & Parrish 1998)

Soil type	K_s (cm/hr)	h_s (cm)	θ_s (cm³/cm³)	θ_{FC} (cm³/cm³)	θ_p (cm³/cm³)	θ_r (cm³/cm³)	α (1/cm)	n
Clay	0.060	31.630	0.380	0.326	0.272	0.068	0.008	1.090
Clay loam	0.20	20.880	0.410	0.318	0.197	0.095	0.019	1.310
Loam	1.320	8.890	0.430	0.27	0.117	0.078	0.036	1.560
Loamy sand	5.980	6.130	0.410	0.125	0.055	0.057	0.124	2.280
Sandy loam	2.180	11.010	0.410	0.207	0.095	0.065	0.075	1.890
Silt loam	0.680	16.680	0.450	0.330	0.133	0.067	0.020	1.410
Silty clay	0.100	29.220	0.360	0.332	0.250	0.070	0.005	1.090
Silty clay loam	0.200	27.30	0.430	0.366	0.208	0.089	0.010	1.230
Sandy clay loam	0.300	21.850	0.390	0.257	0.148	0.100	0.059	1.480

K_s, saturated hydraulic conductivity; h_s, capillary head; θ_s, saturated water content; θ_r, residual water content; n and α, soil water retention parameters; θ_{FC}, field capacity; and θ_p, wilting point
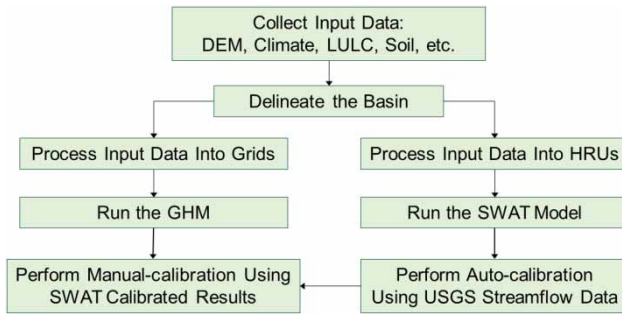
Figure 3 │ Flow chart of the joint hydrologic modeling and cross-calibration for the Red River of the North Basin.

Model comparison and cross-calibration

The SWAT model was run for a 15-year period from 1998 to 2012, with the first five years (1998–2002) as a warm-up period and the remaining 10 years for model calibration. Following Lin *et al.* (2015), 14 SWAT parameters were chosen for model calibration. These parameters, listed in Table 4, represented different hydrologic processes of runoff generation and channel routing in the RRB. SWAT-CUP (Abbaspour 2013), which links SUFI2 (Sequential Uncertainty Fitting, version 2) to SWAT, and the observed streamflow data at 16 USGS gauging stations in the RRB were used for the model calibration. Following Moriasi *et al.* (2007, 2015), two statistics were used to assess the model performance: (1) Nash–Sutcliffe efficiency (NSE)

(Nash & Sutcliffe 1970), which has been widely used to evaluate the performance of hydrologic models, and (2) percent bias (PBIAS), which represents the average tendency of the simulated values to be higher or lower than the observed values. Positive and negative PBIAS values indicate overestimation and underestimation of a model, respectively. The NSE and PBIAS can be respectively expressed as:

$$NSE = 1 - \frac{\sum_{i=1}^{N}(Q_{o,i} - Q_{s,i})^2}{\sum_{i=1}^{N}(Q_{o,i} - \overline{Q_o})^2} \tag{1}$$

$$PBIAS = \frac{\sum_{i=1}^{N}(Q_{s,i} - Q_{o,i})}{\sum_{i=1}^{N}(Q_{o,i})} \times 100 \tag{2}$$

where $Q_{o,i}$ = observed discharge at time step i; $Q_{s,i}$ = simulated discharge at time step i; $\overline{Q_o}$ = mean observed discharge; and N = total number of time steps.

Note that the RRB region has suffered from frequent flooding and drought events in the past decade. Over the study period, historical floods occurred in 2008, 2009, and 2011, followed by an extreme drought event in 2012 (Lin *et al.* 2015). However, this study focused on demonstrating the proposed modeling framework and strategy, instead of examining and showing the capabilities of the GHM to simulate hydrologic extremes. Thus, a 5-year period from 2003 to 2007 (1,826 daily time steps) was selected for the GHM modeling.

Table 4 │ Initial and calibrated values of SWAT parameters

Parameter (unit)	Description	Default value	Calibrated value/range
SURLAG (day)	Surface runoff lag coefficient	4.0	0.2
SFTMP (°C)	Snowfall temperature	1.0	0.0
SMTMP (°C)	Snowmelt temperature	0.5	3.0
TIMP	Snowpack temperature lag factor	1.0	0.5
CN2	SCS runoff curve number	Vary	Vary
CANMX (mm)	Maximum canopy storage	0	10–15
SOLAWC (1) (mm H$_2$O/mm Soil)	Available water capacity of the top layer	Vary	Vary
ALPHA_BF (1/day)	Baseflow recession constant	0.048	0.01–0.95
GW_DELAY (day)	Groundwater delay	31	10
GWQMN (mm H$_2$O)	Threshold depth of shallow aquifer for return flow to occur	1,000	300–1,400
GW_REVAP	Groundwater revap coefficient	0.02	0.02–0.3
RCHRG_DP	Deep aquifer percolation fraction	0.05	0.05–0.2
CH_K1 (mm/h)	Effective hydraulic conductivity in tributary channel alluvium	0.0	0.0–5.0
CH_K2 (mm/h)	Effective hydraulic conductivity in main channel alluvium	0.0	0.0–5.0

Calibration of a macro-scale grid-based model is a challenge. Satellite data can be utilized to calibrate different hydrologic processes (e.g. Lohmann *et al.* 1996; Güntner 2008); however, the temporal and spatial resolutions of such data are often limited. The current study involved two distinct modeling approaches: grid-based GHM and subbasin-based SWAT. It should be noted that this study was not intended to show the superiority of these two methods over each other. Instead, a cross-calibration strategy was implemented in this study to take full advantage of both modeling methods. Specifically, auto calibration of the subbasin-based SWAT model was performed by using SWAT-CUP (Abbaspour 2013) and comparing the SWAT simulations against the observed discharges at the 16 gauging stations. The information from the well-calibrated SWAT was then transferred to the GHM for its calibration. To do so, a cross-model comparison scheme (Figure 4) was designed to relate the different hydrologic processes simulated by the subbasin-based SWAT model to those by the grid-based GHM. As shown in Figure 4, the 178 HUC-10 subbasins in the SWAT model were overlaid with the 6,351 GHM grids, from which the hydrologic quantities (e.g. snowmelt, snowpack water equivalent (SWE), surface runoff, and infiltration) simulated by SWAT were extracted and used to calibrate the GHM. Typically, each subbasin included a number of GHM grids (Figure 4). The major calibration parameters for the GHM included CN,

snowmelt threshold temperature, and initial abstraction coefficient.

In the cross-calibration process, the grid-averaged CN values in the GHM were adjusted to be consistent with the corresponding subbasin CN value in the calibrated SWAT model. This process was repeated for all subbasins and their associated grids in the two models. When simulating snowpack and snowmelt, SWAT used several parameters to account for various factors such as surface topography, snow temperature, and drifting, while GHM adjusted the threshold temperature of snowmelt for each grid to account for heterogeneity. In contrast, SWAT used one value for the snowmelt threshold temperature for the entire basin (see Table 4). The initial abstraction (I_a) in the CN method is generally estimated by $I_a = \alpha S$, in which S is the potential retention and the default initial abstraction coefficient $\alpha = 0.2$. Since the GHM had separate simulations for interception of the canopy zone and the impact of surface depressions, it was logical to calibrate α, instead of using a fixed value of 0.2.

RESULTS AND DISCUSSION

SWAT results

Using the streamflow data observed at the 16 USGS gauging stations in the RRB, 14 SWAT parameters were calibrated
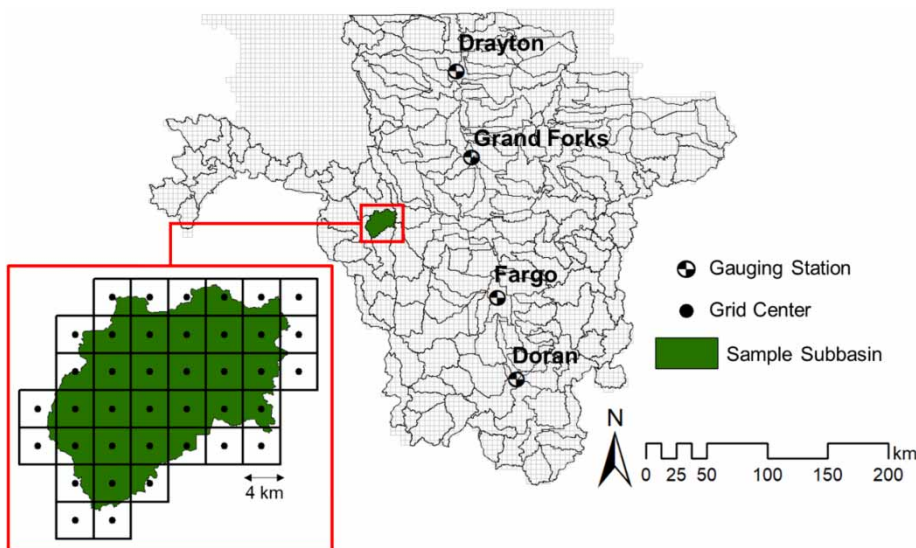

Figure 4 │ Cross-model comparison scheme designed for cross-calibration of the grid-based hydrologic model for the Red River of the North Basin.

(Table 4). Figure 5 shows the calibrated monthly average flows at the Doran (a few miles south to Wahpeton, Figure 2), Fargo, Grand Forks, and Drayton gauging stations (Figure 2) along the main channel of the Red River. Overall, SWAT provided reasonable simulations for low flow conditions at the four stations (Figure 5(a)–5(d)). For high flow conditions, the simulated discharges also matched the observed data very well in terms of both distribution and magnitude for the years before 2009, except for over-predicting three snowmelt events at the upstream Doran station in 2005–2007 (Figure 5(a)). For 2009–2011, however, SWAT failed to capture the peaks caused by the historical extreme floods and underestimated the high flows at the four stations during the flooding periods (Figure 5(a)–5(d)). In addition, a severe drought occurred in the RRB in 2012, resulting in very low streamflow levels. As shown in Figure 5, the simulated monthly average discharges for 2012 were consistently higher than the observed data.

To evaluate the performance of the SWAT model, NSE and PBIAS were also calculated for both monthly average and daily discharges at the four gauging stations along the main channel of the Red River (Table 5). According to Moriasi *et al.* (2007, 2015), NSE values greater than 0.50 and PBIAS values between −25 and +25% indicate an acceptable level of model performance. As shown in Table 5, both NSE and PBIAS demonstrated the good and acceptable performance of the SWAT model for the RRB. It is worth

noting that the SWAT model tended to overestimate the streamflow at Doran whereas it slightly underestimated that at the other three stations (Table 5 and Figure 5). Nevertheless, it can be concluded that the calibrated SWAT model was able to provide acceptable simulations of streamflow in the Red River. In addition to these four stations, NSE and PBIAS were calculated for another 12 stations within the RRB. The results for those 12 stations suggested that the PBIAS values for all stations fell into the acceptable range from −25 to +25%. In addition, eight out of 12 gauging stations had an NSE of greater than 0.6, with the highest NSE of 0.83 for Sand Hill River at Climax, MN.

Joint SWAT-GHM modeling results

The grid-based GHM was cross-calibrated based on the well-calibrated, subbasin-based SWAT simulations. Figure 6 shows the comparisons of four monthly hydrologic variables, including snowmelt, SWE, infiltration, and surface runoff, simulated by the subbasin-based SWAT and the grid-based GHM for the RRB. A visual comparison between the SWAT and GHM results in Figure 6(a)–6(d) indicates that both magnitude and timing of the peaks from the two models are in good agreement. For example, the snowmelt peaks simulated by the SWAT and the GHM for March 2007 were 44.54 and 46.91 mm, respectively (Figure 6(a)) and the snowmelt peaks for other years were also similar.
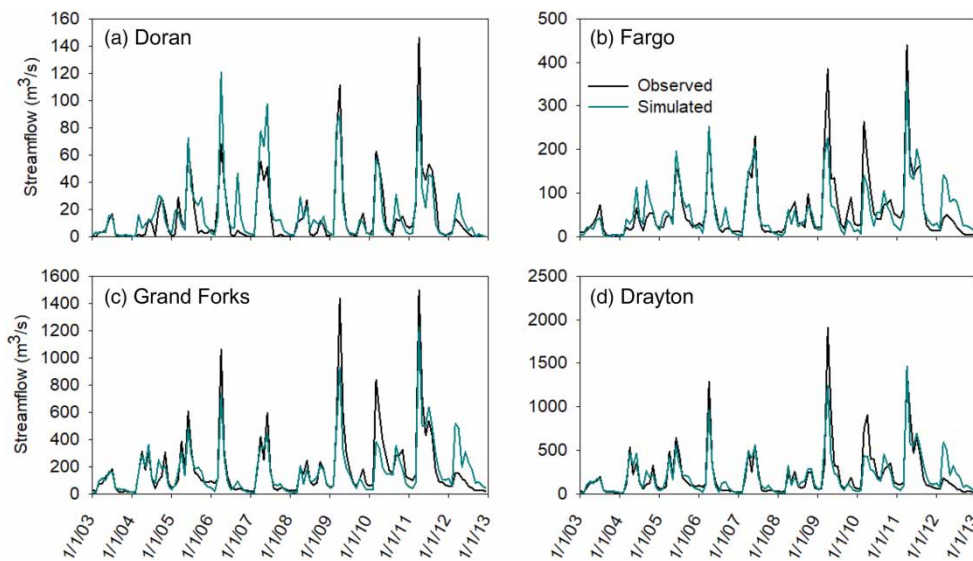

Figure 5 │ Comparisons of the observed and simulated monthly average discharges for four selected stations: (a) Doran, (b) Fargo, (c) Grand Forks, and (d) Drayton.

Table 5 │ NSE and PBIAS values for the SWAT monthly and daily average discharges at four gauging stations along the main channel of the Red River

Statistics	Doran	Fargo	Grand Forks	Drayton
Results for monthly average discharges				
NSE	0.72	0.78	0.79	0.79
PBIAS (%)	18.1	−1.3	−6.6	−0.3
Results for daily average discharges				
NSE	0.58	0.70	0.71	0.79
PBIAS (%)	17.9	−1.3	−6.5	−0.3

For SWE, however, the SWAT peaks occurred earlier than the GHM peaks (Figure 6(b)). This can be attributed to the underlying methodologies used for computing SWE in the two models. Specifically, SWAT utilized an exponential equation to account for the impacts of drifting, shading, and topography on the snow cover within each subbasin, while GHM did not consider these factors and only employed a simple threshold temperature-based approach. The infiltration and surface runoff simulated by SWAT and GHM were also comparable (Figure 6(c) and 6(d)).

Table 6 provides a summary of the four main hydrologic variables (i.e. snowmelt, SWE, infiltration, and surface runoff) simulated by the SWAT and the GHM for the RRB. For the 5-year simulation period, the differences of the yearly values were less than 17%, except for the SWE in 2003–2004 and the snowmelt in 2003. The differences between the annual averages of the four hydrologic variables ranged from 3.87 to 16.43%.

GHM cross-calibrated results

Figure 7 depicts the spatial distributions of rainfall, surface runoff, and infiltration over the RRB on July 7, 2004. The average rainfall over the entire RRB was 13 mm and the southern and eastern parts of the basin received more rainfall than the northwestern basin (Figure 7(a)). The average surface runoff over the RRB was 1.62 mm on July 7, 2004, and more surface runoff was generated in the middle and southern parts of the basin (Figure 7(b)). This trend can be directly attributed to the spatial distribution of CN values controlled by soil types and LULC in the RRB. For example, the dominant silty clay soil and the high percentage of impervious land surfaces in the area close to Fargo led to a much higher amount of surface runoff (24.6 mm). Figure 7(c) illustrates the distribution of infiltration over the RRB and the average infiltration over the basin on July 7, 2004 was 10.84 mm. A visual comparison between Figure 7(a) and 7(c) suggests that rainfall and infiltration followed a similar spatial distribution pattern where both decreased from southeast to northwest.

Snow accumulation and snowmelt are prominent hydrologic processes in the RRB in winters. Figure 8(a)–8(f)
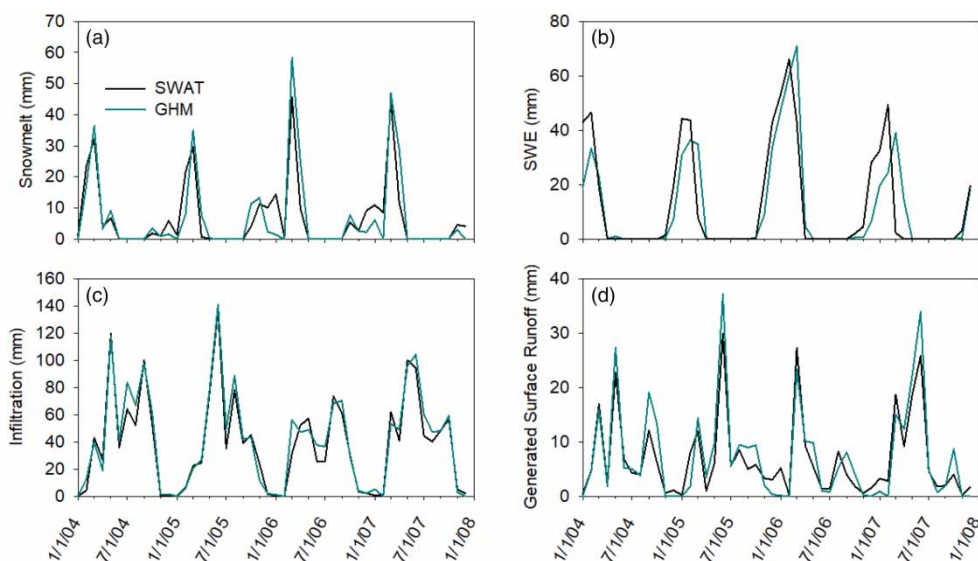

Figure 6 │ Comparisons of four monthly hydrologic variables simulated by the subbasin-based SWAT and the grid-based hydrologic model (GHM) for the Red River of the North Basin: (a) snowmelt, (b) snowpack water equivalent (SWE), (c) infiltration, and (d) surface runoff.

Table 6 │ Comparisons of four main water balance terms (snowmelt, snowpack water equivalent, infiltration, and surface runoff) simulated by the SWAT and the grid-based hydrologic model (GHM) for the Red River of the North Basin

Process	Model	2003	2004	2005	2006	2007	Annual Average
Snowmelt (mm)	GHM	57.64	72.48	78.10	97.08	85.15	78.09
	SWAT	78.44	76.36	78.81	87.92	84.64	81.23
	Difference (%)	26.51	5.08	0.90	10.42	0.59	3.87
Snowpack Water Equivalent (mm)	GHM	2.23	6.99	12.15	15.91	9.66	9.39
	SWAT	6.76	10.76	13.35	16.42	8.89	11.24
	Difference (%)	66.98	34.97	8.98	3.09	8.61	16.43
Infiltration (mm)	GHM	412.45	542.67	511.10	402.20	525.61	478.81
	SWAT	385.10	501.34	490.41	364.85	496.57	447.65
	Difference (%)	7.09	8.24	4.22	10.23	5.84	6.95
Surface Runoff (mm)	GHM	43.27	96.35	102.64	63.13	100.83	81.24
	SWAT	47.16	82.54	88.55	66.59	92.77	75.52
	Difference (%)	8.25	16.73	15.90	5.20	8.68	7.57
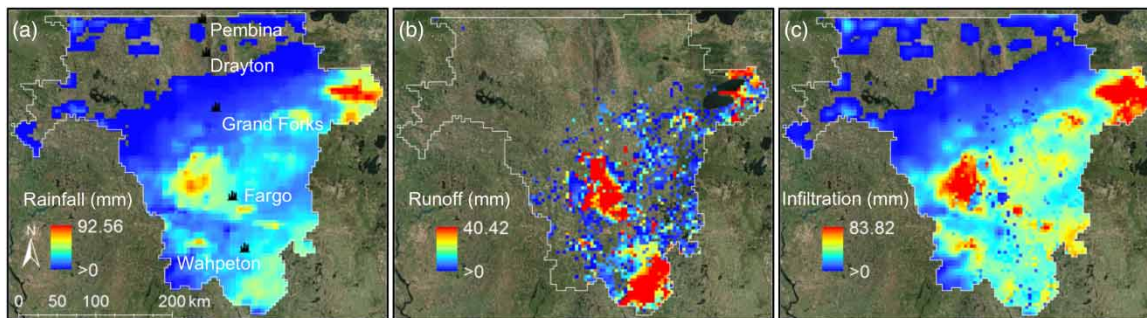
Figure 7 │ Spatially distributed results simulated by the grid-based hydrologic model on July 7, 2004: (a) rainfall, (b) surface runoff, and (c) infiltration.

exemplify the spatial distributions of snowpack SWE and snowmelt over the RRB for three selected dates: January 22, March 22, and March 29, 2005. Figure 8(a)–8(c) display a progressively decreasing trend of the snowpack SWE from southwest to northeast on the three selected days in 2005. The average snowpack SWE values were 39.08, 39.14, and 22.74 mm on January 22, March 22, and March 29, respectively. Understandably, these variations were mainly affected by the variations in temperature. The average temperatures on March 22 varied from +2.86 °C in Wahpeton (south) to −3.12 °C in Pembina (north), resulting in a reduction in snowpack depth in the southern part of the basin. In addition, Figure 8(d)–8(f) reveal the snowmelt trend in the RRB. The snow-melting process started from the southwestern side of the basin and moved towards the northeastern side (Figure 8(d)–8(f)). The average snowmelt over the

RRB on January 22, March 22, and March 29 was 0, 0.19, and 7.89 mm, respectively.

In addition to the surface hydrologic processes, the GHM also provided simulation results for subsurface processes. Figure 9(a) and 9(b) show the spatial distribution of topsoil water storage (TWS) in the RRB on January 1, 2006 and April 2, 2006, respectively. The average TWS for the entire basin on January 1, 2006 was 67.44 mm, whereas it increased to 78.89 mm on April 2, 2006. This trend also occurred for all other years, which can be mainly attributed to the spring snowmelt as a direct result of higher temperature in March and April. Figure 9(a) and 9(b) also reveal a spatial pattern which affected surface runoff and infiltration. A closer look at the red box in Figure 9(b) indicates that the middle part of the basin along the Red River Valley accounted for the higher TWS values due to the silty clay and silty clay loam soils in the Red River valley. This unique soil distribution
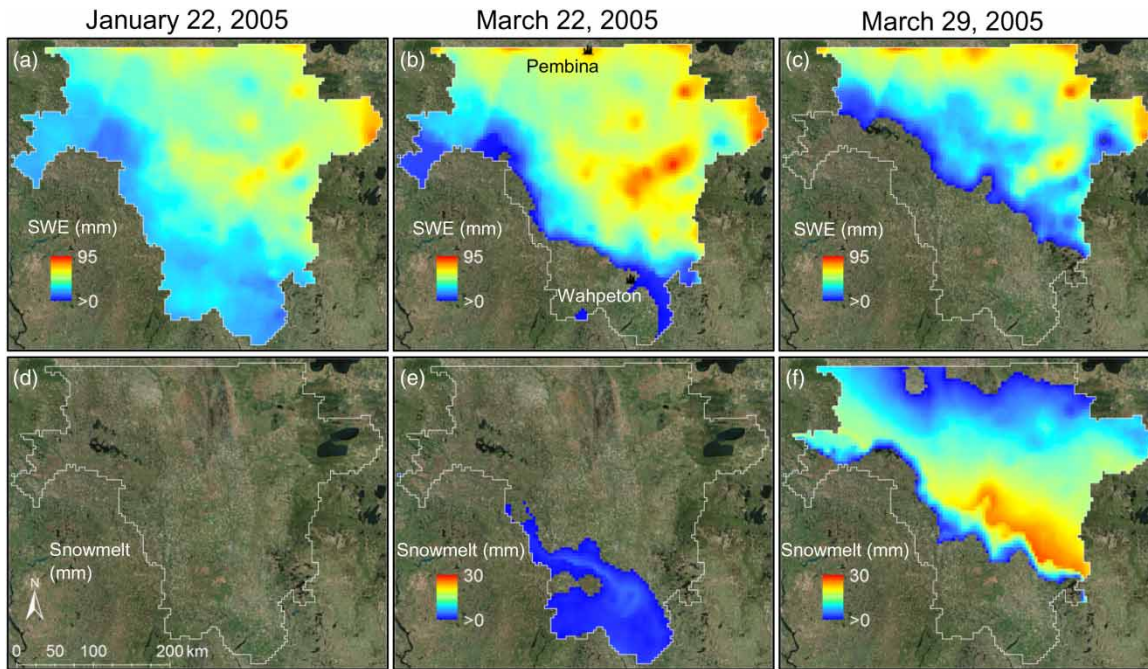
Figure 8 │ Spatially distributed snowpack water equivalent (SWE) depth and snowmelt simulated by the grid-based hydrologic model for three selected dates: January 22, 2005 (a) and (d); March 22, 2005 (b) and (e); and March 29, 2005 (c) and (f).
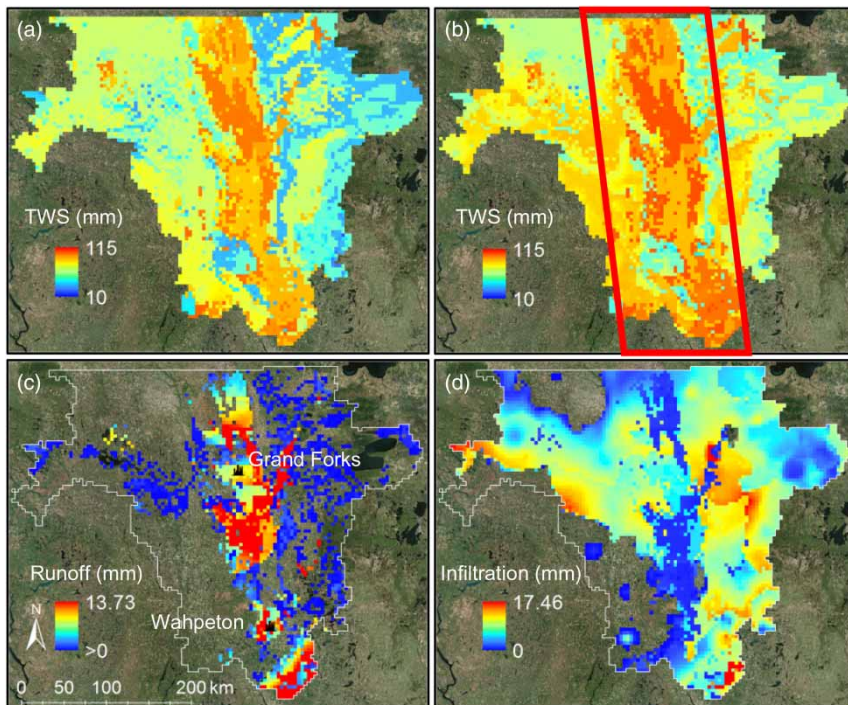

Figure 9 │ Spatially distributed (a) and (b) topsoil water storage (TWS), (c) surface runoff, and (d) infiltration simulated by the grid-based hydrologic model for two selected dates: (a) January 1, 2006; and (b)–(d) April 2, 2006.
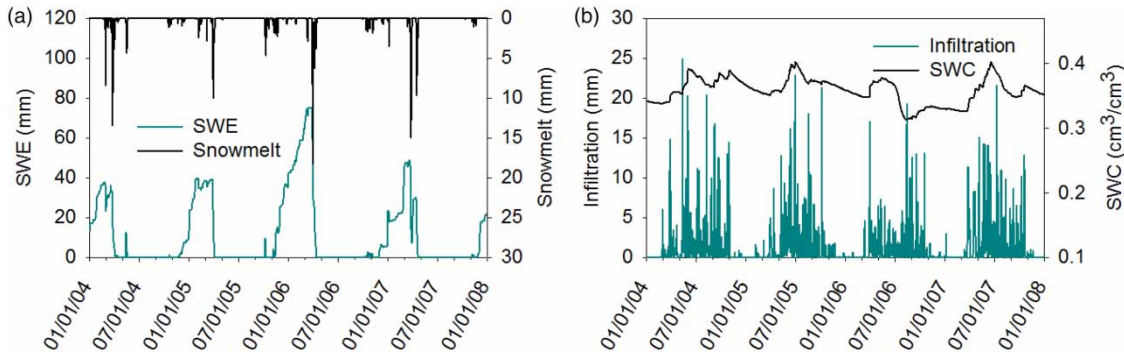
Figure 10 | Temporal distributions of (a) average snowmelt and snowpack water equivalent (SWE) and (b) average infiltration and root zone soil water content (SWC) simulated by the grid-based hydrologic model for the Red River of the North Basin.

also impacted infiltration and surface runoff. Figure 9(c) and 9(d) highlight the spatially distributed surface runoff and infiltration on April 2, 2006. It can be observed that more runoff was generated, and less water infiltrated into soils along the Red River Valley. The average surface runoff for the entire basin on April 2, 2006 was 0.48 mm; however, the surface runoff values in the areas of Wahpeton and Grand Forks, dominated by silty clay and silty clay loam soils, were as high as 4.23 and 2.67 mm, respectively.

The GHM can also be used to simulate the temporal distributions of hydrologic processes for the entire basin to reveal basin-wide trends. Figure 10(a) shows the basin-wide average snowmelt and SWE, indicating that most snowmelt peaks occurred right after the corresponding SWE peaks. For example, the maximum average SWE occurred on March 25, 2006, which was followed by the maximum average snowmelt on March 30, 2006. Moreover, Figure 10(b) shows the variations in the average infiltration and the soil water content (SWC) of the root zone. The SWC peaks coincided with the infiltration peaks. SWC varied within a range of 0.36–0.42 cm^3/cm^3.

CONCLUSIONS

In this study, a macro-scale modeling framework was proposed for joint simulation and cross-calibration of a new GHM and the widely-used SWAT model. This modeling strategy was applied to the RRB. A two-step cross-calibration procedure was developed, which involved (1) direct calibration of the subbasin-based SWAT model using the observed streamflow data and (2) indirect calibration of the GHM by transferring the well-calibrated, subbasin-based SWAT simulations to the GHM grids. The simulation results from the two models were analyzed and compared. The performance of the SWAT model was quantitatively assessed by the NSE and PBIAS for the simulated and observed hydrographs. The NSE values were greater than 0.5 and the PBIAS values were within a range of ±25%, showing acceptable model performance.

This study presented a new way of calibrating a macro-scale GHM by taking full advantage of two different modeling structures and approaches. The simulation results demonstrated the feasibility of the two-step cross-calibration procedure that combined the subbasin-based and grid-based modeling methodologies, as well as the capability of the GHM in grid-based simulations of surface runoff, infiltration, snowmelt, and other hydrologic processes. Some discrepancies in the simulations from the subbasin-based SWAT and grid-based GHM can be mainly attributed to the differences in the modeling methods used in the two models for specific hydrologic processes.

The gridded simulation results from the calibrated macro-scale GHM can be used to better understand the localized (up to a grid) hydrologic processes (e.g. overland flow generation, infiltration, depression storage, snowpack, snowmelt, soil moisture condition, and subsurface flow), and further analyze their variations across space and time, as well as their spatio-temporal trends at a macro scale. The joint modeling framework, grid-based hydrologic modeling method, and the two-step cross-calibration procedure developed in this study can be readily applied

to other macro-scale basins. Although this cross-calibration approach makes the calibration of the macro-scale, grid-based model much easier, there are some limitations. Caution should be taken if this method is used for very large grids that might not fit into subbasin boundaries. In addition, the uncertainties related to the subbasin-based SWAT model can be transferred to the GHM.

ACKNOWLEDGEMENTS

REFERENCES

Abbaspour, K. C. 2013 *SWAT-CUP 2012: SWAT Calibration and Uncertainty Program – A User Manual*. EAWAG: Swiss Federal Institute of Aquatic Science and Technology, Dübendorf, Switzerland.

Allen, R. G., Pereira, L. S., Raes, D. & Smith, M. 1998 *Crop Evapotranspiration: Guidelines for Computing Crop Requirements. FAO Irrigation Drainage Paper 56*. Food and Agriculture Organization of the United Nations, Rome, p. 300.

Bell, V. A., Kay, A. L., Jones, R. G. & Moore, R. J. 2007 Development of a high resolution grid-based river flow model for use with regional climate model output. *Hydrol. Earth Syst. Sci.* 11 (1), 532–549.

Bennett, T. 1998 *Development and Application of A Continuous Soil Moisture Accounting Algorithm for the Hydrologic Engineering Center Hydrologic Modeling System (HEC-HMS)*. MS Thesis, Dept of Civil and Environmental Engineering, University of California, Davis, California.

Blöschl, G. & Sivapalan, M. 1995 Scale issues in hydrological modelling: a review. *Hydrol. Process.* 9 (3–4), 251–290.

Blöschl, G., Ardoin-Bardin, S., Bonell, M., Dorninger, M., Goodrich, D., Gutknecht, D., Matamoros, D., Metz, B., Shand, P. & Szolgay, J. 2007 At what scales do climate variability and land cover change impact on flooding and low flows? *Hydrol. Process.* 21 (9), 1241–1247.

Carsel, R. F. & Parrish, R. S. 1988 Developing joint probability distributions of soil water retention characteristics. *Water Resour. Res.* 24 (5), 755–769. https://doi.org/10.1029/WR024i005p00755.

Chu, X., Yang, J., Chi, Y. & Zhang, J. 2013 Dynamic puddle delineation and modeling of puddle-to-puddle filling-spilling-merging-splitting overland flow processes. *Water Resour. Res.* 49 (6), 3825–3829.

Daly, C., Halbleib, M., Smith, J. I., Gibson, W. P., Doggett, M. K., Taylor, G. H., Curtis, J. & Pasteris, P. P. 2008 Physiographically sensitive mapping of climatological temperature and precipitation across the conterminous United States. *Int. J. Climatol.* 28 (15), 2031–2064.

Daly, C., Smith, J. I., Olson, K. V., Smith, J., Gibson, W. & Senay, G. 2015 Mapping atmospheric moisture climatologies across the conterminous United States. *PLOS ONE* 10 (10), e0141140.

Dile, Y. T. & Srinivasan, R. 2014 Evaluation of CFSR climate data for hydrologic prediction in data-scarce watersheds: an application in the Blue Nile River Basin. *Journal of the American Water Resources Association* 50 (5), 1226–1241. https://doi.org/10.1111/jawr.12182.

Döll, P., Berkhoff, K., Bormann, H., Fohrer, N., Gerten, D., Hagemann, S. & Krol, M. 2008 Advances and visions in large-scale hydrological modelling: findings from the 11th Workshop on Large-Scale Hydrological Modelling. *Adv. Geosci.* 18, 51–61.

Douglas-Mankin, K. R., Srinivasan, R. & Arnold, J. G. 2010 Soil and Water Assessment Tool (SWAT) model: current developments and applications. *Trans. ASABE* 53 (5), 1423–1431.

ESRI 2011 *ArcGIS Desktop*: Release 10. Environmental Systems Research Institute, CA.

Flint, L. E., Flint, A. L., Thorne, J. H. & Boynton, R. 2013 Fine-scale hydrologic modeling for regional landscape applications: the California Basin Characterization Model development and performance. *Ecol. Process.* 2 (1), 1–21.

Fry, J. A., Xian, G., Jin, S., Dewitz, J. A., Homer, C. G., Yang, L., Barnes, C. A., Herold, N. D. & Wickham, J. D. 2011 Completion of the 2006 national land cover database for the conterminous united states. *Photogramm. Eng. Remote Sensing* 77 (9), 858–864.

Galloway, J. M., Blanchard, R. A. & Ellison, C. A. 2011 *Sediment Concentrations, Loads, and Particle-Size Distributions in the Red River of the North and Selected Tributaries Near Fargo, North Dakota, During the 2011 Spring High-Flow Event*. US Geological Survey Scientific Investigations Report 2011-5064, Reston, Virginia, p. 27.

Green, W. H. & Ampt, G. A. 1911 Studies on soil physics. *J. Agric. Sci.* 4 (1), 1–24.

Gudmundsson, L., Tallaksen, L. M., Stahl, K., Clark, D. B., Dumont, E., Hagemann, S., Bertrand, N., Gerten, D., Heinke, J., Hanasaki, N., Voss, F. & Koirala, S. 2012a Comparing large-scale hydrological model simulations to observed runoff percentiles in Europe. *J. Hydrometeorol.* 13 (2), 604–620.

Gudmundsson, L., Wagener, T., Tallaksen, L. M. & Engeland, K. 2012b Evaluation of nine large-scale hydrological models with respect to the seasonal runoff climatology in Europe. *Water Resour. Res.* 48 (11), 1–20.

Güntner, A. 2008 Improvement of global hydrological models using GRACE data. *Surv. Geophys.* 29 (4–5), 375–397.

Habtezion, N., Tahmasebi Nasab, M. & Chu, X. 2016 How does DEM resolution affect microtopographic characteristics,

hydrologic connectivity, and modeling of hydrologic processes? *Hydrol. Process.* **30** (25), 4870–4892.

Hargreaves, G. H. & Samani, Z. A. 1985 Reference crop evapotranspiration from temperature. *Appl. Eng. Agric.* **1** (2), 96–99.

Hasan, S., Montzka, C., Rüdiger, C., Ali, M., Bogena, H. R. & Vereecken, H. 2014 Soil moisture retrieval from airborne L-band passive microwave using high resolution multispectral data. *ISPRS J. Photogramm. Remote Sensing* **91**, 59–71.

Jin, C. X., Sands, G. R., Kandel, H. J., Wiersma, J. H. & Hansen, B. J. 2008 Influence of subsurface drainage on soil temperature in a cold climate. *J. Irrig. Drain. Eng.* **134** (1), 83–88.

Krysanova, V. & Arnold, J. G. 2008 Advances in ecohydrological modelling with SWAT – a review. *Hydrol. Sci. J.* **53** (5), 939–947.

Liang, X., Lettenmaier, D. P., Wood, E. F. & Burges, S. J. 1994 A simple hydrologically based model of land surface water and energy fluxes for general circulation models. *J. Geophys. Res.* **99** (D7), 14415–14428.

Lin, Z., Anar, M. J. & Zheng, H. 2015 Hydrologic and water-quality impacts of agricultural land use changes incurred from bioenergy policies. *J. Hydrol.* **525**, 429–440.

Lohmann, D., Nolte-Holube, R. & Raschke, E. 1996 A large-scale horizontal routing model to be coupled to land surface parametrization schemes. *Tellus A* **48** (5), 708–721.

Maidment, D. R. 1993 *Handbook of Hydrology*. McGraw-Hill Education, New York.

Mohammed, G. a., Hayashi, M., Farrow, C. R. & Takano, Y. 2013 Improved characterization of frozen soil processes in the Versatile Soil Moisture Budget model. *Can. J. Soil Sci.* **93**, 511–531.

Monteith, J. L. 1965 Evaporation and the environment in the state and movement of water in living organisms. In: *Proceedings of the Society for Experimental Biology, Symposium No. 19*. Cambridge University Press, Cambridge, pp. 205–234.

Moriasi, D. N., Arnold, J. G., Van Liew, M. W., Bingner, R. L., Harmel, R. D. & Veith, T. L. 2007 Model evaluation guidelines for systematic quantification of accuracy in watershed simulations. *Trans. ASABE* **50** (3), 885–900.

Moriasi, D. N., Zeckoski, R. W., Arnold, J. G., Baffaut, C., Malone, R. W., Daggupati, P., Guzman, J. A., Saraswat, D., Yuan, Y., Wilson, B. N., Shirmohammadi, A. & Douglas-Mankin, K. R. 2015 Hydrologic and water quality models: key calibration and validation topics. *Trans. ASABE* **58** (6), 1609–1618.

Nash, J. E. & Sutcliffe, J. V. 1970 River flow forecasting through conceptual models part I – a discussion of principles. *J. Hydrol.* **10** (3), 282–290.

Neitsch, S. L., Arnold, J. G., Kiniry, J. R. & Williams, J. R. 2011 *Soil and Water Assessment Tool (SWAT) Theoretical Documentation, Version 2009*. Texas Water Resources Institute, College Station, Texas.

NRCS 2017 *SSURGO Database*. Natural Resources Conservation Service, United States Department of Agriculture. Available from: https://websoilsurvey.sc.egov.usda.gov (April 27, 2017).

Paiva, R. C. D., Collischonn, W. & Tucci, C. E. M. 2011 Large scale hydrologic and hydrodynamic modeling using limited data and a GIS based approach. *J. Hydrol.* **406** (3), 170–181.

Planchon, O. & Darboux, F. 2002 A fast, simple and versatile algorithm to fill the depressions of digital elevation models. *CATENA* **46** (2), 159–176.

Priestley, C. H. B. & Taylor, R. J. 1972 On the assessment of surface heat flux and evaporation using large-scale parameters. *Mon. Weather Rev.* **100** (2), 81–92.

Rawls, W. J., Brakensiek, D. L. & Saxtonn, K. E. 1982 Estimation of soil water properties. *Transactions of the ASAE* **25** (5), 1316–1320. doi: 10.13031/2013.33720.

Rawls, W. J. & Brakensiek, D. L. 1983 A procedure to predict Green and Ampt infiltration parameters. In: *Advances in infiltration: proceedings of the National Conference on Advances in Infiltration*, American Society of Agricultural Engineers, St. Joseph, Michigan, pp. 102–112.

Red River Basin Board 2000 *Inventory Team Report: Hydrology*. Red River Basin Board, Moorhead, MN.

Samaniego, L., Kumar, R. & Attinger, S. 2010 Multiscale parameter regionalization of a grid-based hydrologic model at the mesoscale. *Water Resour. Res.* **46** (5), 1–25.

Schwert, D. P. 2009 *What Makes the Red River of the North So Vulernable to Flooding?* Available from: www.ndsu.edu/fargo_geology/whyflood.htm (November 8, 2016).

Sood, A. & Smakhtin, V. 2015 Global hydrological models: a review. *Hydrol. Sci. J.* **60** (4), 549–565.

Stadnyk, T., Dow, K., Wazney, L. & Blais, E.-L. 2016 The 2011 flood event in the Red River Basin: causes, assessment and damages. *Can. Water Resour. J.* **41** (1–2), 65–73.

Suárez, L. A. 2005 *PRZM-3, A Model for Predicting Pesticide and Nitrogen Fate in the Crop Root and Unsaturated Soil Zones: Users Manual for Release 3.12. 2*. US Environmental Protection Agency, Washington, DC.

Tahmasebi Nasab, M., Singh, V. & Chu, X. 2017 SWAT modeling for depression-dominated areas: how do depressions manipulate hydrologic modeling? *Water* **9** (1), 1–14.

Tesfa, T. K., Ruby Leung, L., Huang, M., Li, H.-Y., Voisin, N. & Wigmosta, M. S. 2014 Scalability of grid- and subbasin-based land surface modeling approaches for hydrologic simulations. *J. Geophys. Res. Atmos.* **119** (6), 3166–3184.

USDA 1986 *Urban Hydrology for Small Watersheds*. Technical Release 55 (TR-55). United States Department of Agriculture, Washington, DC.

Winchell, M., Srinivasan, R., Di Luzio, M. & Arnold, J. 2013 *ArcSWAT Interface for SWAT2012: User's Guide*. Blackland Research and Extension Center, Texas Agrilife Research. Grassland. Soil and Water Research Laboratory, USDA Agricultural Research Service, Texas.